Catalysis Science & Technology

Accepted Manuscript

ROYAL SOCIETY OF CHEMISTRY

www.rsc.org/catalysis

A reusable material with high performance for removing NO at room temperature: its performance, mechanism and kinetics

Pei Lu[1], Yi Xing[1*], Caiting Li[2*], Renpeng Qing[2&], Wei Su[1], Nian Liu[3]

[1]School of Civil and Environmental Engineering, University of Science and Technology Beijing, Beijing, 100083, China

[2]College of Environmental Science and Engineering, Hunan University, Changsha 410082, China

[3]Faculty of Environmental Sciences，Dresden University of Technology，Dresden,01069, Germany

*Corresponding author: cnlupei@163.com, xing_bkd@163.com and ctli@hnu.edu.cn. &:The author contribute equally to the first author.

Abstract: Up to now, it is a very challenging work to purify NO by a reusable sample at room temperature. In this study, series materials of urea-MnO_x/ACF and urea-xCeO_2-(1-x)MnO_2/ACF were prepared used for purifying NO at room temperature for the first time. The experimental results showed that 10%urea-8%(0.5CeO_2-0.5MnO_2)/ACF could yield the highest NO conversion among all of the prepared samples, which showed an above 90% NO conversion ratio with 1000 ppm NO in the initial mixed gases. Moreover, its NO conversion could even over 98% when the NO concentration was 100 ppm in the initial mixed gases. What is more important, the stability of 10%urea-8%(0.5CeO_2-0.5MnO_2)/ACF was desirable even it was regenerated by reloading urea, which illustrated that the sample could be easily reused and its high-performance was maintained. Finally, the mechanism and kinetics of the purified process of NO was discussed.

Keyword: NO, ACF, room temperature, catalysis, mechanism and kinetics

1. Introduction

NO_x pollution has seriously affected people's health especially in developing countries. Much attention has been paid on purifying NO_x from flue gas and many promising solutions were reported [1, 2]. Selective catalysis reduction (SCR) of NO with NH_3 is the most widely used method by researchers in the past decades due to its high efficiency [1, 3-4]. A series of catalysts including noble metals [5-7], transition metal oxides [8-12], rare earth oxides [13-15], and metal modified zeolites [3, 16-17] have been used in the control of NO emission. The catalytic activity of these catalysts was high, and desirable NO removal rate could be achieved. However, the experimental temperatures for these catalysts were usually above 120°C and were mainly used for the removal of NO_x in industrial flue gases at elevated temperature. [13, 18]. For the control of NO pollution near traffics cross-section and along high ways where the temperature was ambient temperature (set as 30°C in this study), the catalysts mentioned above would not be active enough to attain high NO conversion

under these conditions.

Transition metal oxides based catalysts [1, 9, 11-13, 19-20], manganese oxides and ceria, were reported to be promising in the application of NO control under ambient condition. With the redox cycle between Mn^{4+} and Mn^{3+}, the Mn-containing catalysts showed high catalytic activity at ambient condition by transferring the electron easily. Meanwhile, the reaction between CeO_2 and Ce_2O_3 could release oxygen which could promote the oxidation of NO to NO_2. In addition, when mixed with manganese oxide, ceria was found to fortify the oxygen storage capability of MnO_x and greatly improve oxygen migration speed for the heterogeneous catalysis [1, 21-25]. Therefore the synergistic effect between the two metal oxides could greatly improve the catalytic efficiency in the SCR process of NO.

Up to now, the control of the NO pollution at room temperature was mainly through several methods: photo-catalytic oxidation by TiO_2 [26-27], biological oxidation [28], and adsorption by carbon material [29]. While photo-catalysts were too expensive for the present NO control and biological oxidation was not suitable for urban NO pollution caused by vehicle release. Physical adsorption by activated carbon material combining with catalytic reaction by metal oxides loaded on carbon materials would be the most suitable for urban NO control at room temperature[30]. Owing to its large specific surface area and special pore-diameter distribution, activated carbon fiber has been widely used in air purification [2, 31]. Urea was reported [32, 33] to be one of the most practical reducing reagents for SCR system ascribing to its high reaction activity with NO_x at low temperature.

It has been considered as an effective way [18, 34-36] for urea supporting on heterogeneous catalysts in the reduction of NO to N_2. Based on our earlier work, we want to find a reusable material with high performance for removing NO at room temperature. In this study, a series of 10%urea-MnO_x/ACF and 10%urea-xCeO_2-(1-x)MnO_2/ACF materials were prepared for NO purification at room temperature and their performance, mechanism and kinetics were studied.

2. Experimental

2.1. Samples preparation

The rayon based ACF, used as catalyst carrier in this study, was supplied by Sutong Carbon Fiber Company. The ACF were first washed by deionized water and then dried at 105°C for 4 h in a drying even (DHG-9023A, Shanghai Qin Mai instrument Co., Ltd). Then, the obtained sample was put in clean and hermetic bags for further use.

The catalysts were prepared through equal-volume impregnation method. The ACF was dipped into a series of certain concentration of $Mn(AC)_2$ solution for 2 h, where mass fraction for MnO_2 were 5%, 8%, 10% and 12% (wt%) , respectively. Then the samples were dried at 105°C and pyrolyzed at 420 °C for 2 h in N_2 stream. Subsequently, the catalysts were grinded to powder, then dipped into 10% (wt %) urea solution for 24 h. After that, the samples were dried at 50°C in a vacuum oven, as got the urea-MnO_x/ACF series samples.

By similar method, the variable mass ratios (1:3, 1:2, 1:1, 2:1and 3:1) of CeO_2 and MnO_x were deposited onto ACF through co-impregnation method, and then were loaded with urea. 10%urea- $xCeO_2$-(1-x)MnO_2/ACF were prepared in this paper. For 10%urea- $xCeO_2$-(1-x)MnO_2/ACF, its total mass percentage of the loaded oxides was 8%, in which *x* and *1-x* refer to the mass ratio of MnO_2 and CeO_2, respectively.

2.2. Measurement of catalytic activity

The experiments of urea-SCR of NO were carried out in a test tube with 20mm in diameter. In the test tube, the powder sample was loaded but not packed. 0.5000g of sample was loaded in the test tube during each experiment. The experiment was carried out under the following condition: gas velocity, 10000 h^{-1}; NO, 1000 ppm; O_2, 21%; N_2, balanced; total flow rate, 225 ml/min; temperature, 30 °C; relative humidity, 0%. The NO concentrations were tested continuously by NO analyzer (Kane Auto5-1, UK) at the inlet and outlet. The NO_2 detected at the outlet was converted to NO to obtain the final NO conversion rate. The influence of NO concentration on the conversion of NO was studied in the test as the previous study [34, 36]. The activity of the sample was

evaluated by the NO conversion rate which was calculated through the following equation:

$$\text{NO conversion}\% = \frac{NO_{x\,inlet} - NO_{x\,outlet}}{NO_{x\,inlet}} \times 100\%$$

2.3. Catalytic characterization

Specific surface area, pore volume and pore diameter were analyzed with an ASAP 2020 apparatus. The X-ray photoelectron spectroscopy (XPS) analyses were performed at room temperature by a K-Alpha 1063 Spectrometer (Thermo Fisher Scientific, UK), with an Al Kα anode (1486.6eV) radiation being operated at 15 KV and 6mA. The powder X-ray diffraction (XRD) patterns were obtained by using a Siemens D5000 system (German) with Cu Kα radiation in continuous scan mode from 10° to 80° of 2θ with 0.02° per second sampling interval. The scanning electron microscope (SEM) (JEOL 6701F) was used to investigate the morphology of the prepared sample. Infrared spectra were recorded on a Compact Fourier transform infrared spectrophotometer (FTIR) (IRAffinity-1, Shimadzu Scientific Instruments, Japan).

3. Results and discussion

3.1. Removal of NO by urea-MnO_x/ACF and urea- $xCeO_2$-(1-x)MnO_2/ACF

Figure 1(a) showed the NO removal plane by 10% urea-MnO_x/ACF. The NO conversion ratio was greatly affected by the loading mass of MnO_x. With the mass ratio of MnO_x increased from 5% to 8%, NO removal plane extended to the higher leval and reached its top when the loading ratio for MnOx was 8% suggesting highest NO removal rate by series 10% urea-MnO_x/ACF samples. After that, the removal plane slowly turned to the low level, indicating the decreased catalytic activity. The NO removal plane by a series of 10%urea-xCeO_2-(1-x)MnO_2/ACF was shown in Figure 1(b). The removal ratio of NO was 75% when mass ratio of CeO_2 and MnO_x was 1:3, which showed its superiority compared to the samples with MnO_x supported alone. As the mass ratio of CeO_2 and MnO_x changed from 1:3 to 1:1, the removal plane upswings implying the increased NO conversion rate. When the mass ratio of CeO_2 and

MnO_x was 1:1, the plane reach the zenith, signifying the highest NO removal, up to 90%, by 10%urea- $xCeO_2$-(1-x)MnO_2/ACF. As the mass ratio of CeO_2 and MnO_x changed from 1:1 to 1:3, the NO removal plane declined to the lower leval accompanied with the decreased NO conversion rate. The results was consistent with previous research [36]. Compared with the 10%urea-CeO_2-CuO/ACF samples reported in our previous paper [36], 10%urea- 0.5CeO_2-0.5MnO_2/ACF could yield higher NO removal when the mass ratio of two metal oxides was 1:1.

3.2. Catalytic stability experiments

Figure 2 showed the catalytic stability of 0.5000 g 10%urea-0.5CeO_2-0.5MnO_2/ACF under the condition of 1000 ppm NO and 21% O_2 concentration at 30**℃**. It could be seen from Figure 2 that the sample could remain over 85% NO conversion in the first 3 h, and then the NO conversion rate slowly dropped from 85% to 75% in the next hour. After that, the conversion rate of NO dropped quickly.

When urea was reloaded onto material of 10%urea-0.5CeO_2-0.5MnO_2/ACF after 4 hours' reaction in the SCR system, its reactivity was recovered and the NO conversion ratio was scarcely affected. It demonstrated that the material could be reused after an oversimplified and feasible treatment while its purification capacity could almost unaffected.

3.3. Effect of NO concentration

Figure 3 showed the performance of 10%urea-0.5CeO_2-0.5MnO_2/ACF in different NO concentrations (100 ppm, 200 ppm, 500 ppm, 1000 ppm).

When the concentration of NO was 100 ppm, over 98% NO conversion could be achieved, which was apparently much higher than those in other NO concentrations. When the NO concentration increased to 500 ppm, the NO conversion rate decreased from 98% to 87%. In contrast, when the NO concentration increased from 500 ppm to 1000 ppm, the removal of NO increased. Previous research on the reaction of NO with urea loaded on activated carbons fiber reported that when NO concentration increased

from 100 ppm to 1000 ppm, the conversion increased continuously [37], but without detailed explanation. In this paper, the effect of NO concentration on its conversion will be detailed discussed in later paragraphs.

3.4. BET study

The surface areas, total pore volumes (V_t), micro-pore volume, and pore size of ACF, 10%urea-5%MnO_x/ACF, 10%urea-8%MnO_x/ACF, 10%urea-10%MnO_x/ACF and 10% urea-0.5CeO_2-0.5MnO_2 /ACF were summarized in Table 1.

It could be found that there was an apparent change of surface area, micro-pore volume (V_{micro}) and pore diameters (D_A) with urea and different mass ratios of manganese and cerium oxides loaded on ACF. With the increase in the loading amount of manganese oxide, the surface area of the sample declined rapidly. However, the mesoporous surface area (S_{meso}) of the sample increased a certain amount before dropping. And the microporous area (S_{micro}) varies with the changing in the loading amount of manganese oxide. This phenomenon might be ascribed to the dispersion of manganese and cerium oxides which might filled in the mesoporous and therefore leading to the transformation of certain amount of mesoporous to microporous. [36,38] Meanwhile, new interconnecting pores might emerge.[38] All these would result in the change of S_{micro}. Combined with the NO conversion rates in Fig. 1, it could be found that the increase of S_{micro}, as well as the increase of the ratio of V_{micro} to V_t, might be beneficial to increase the NO conversion [13].

3.5. XPS study

To confirm the oxidation state of the metal oxide loaded on ACF and to understand the catalytic mechanism in the NO conversion process, XPS characterizations of 10%urea-8% MnO_x/ACF and 10%urea-0.5CeO_2-0.5MnO_2/ACF were studied.

Table 2 showed the surface atomic concentrations of Mn, Ce, O and N. The results showed that the atomic ratio of manganese and cerium on the surface of ACF was less than 1:1. It might be the reason that cerium oxides were dispersed on the surface of ACF, while more manganese oxides were bedded in the mesoporous of ACF [36].

Figure 4(a) showed the binging energy peaks of the Mn 2p in 10%urea-8%MnO_x/ACF which suggested the coexistence of Mn^{4+} and Mn^{3+}. In Fig. 3(a), it could be seen that Mn^{3+} was at 2p 3/2 and 2p 1/2 with the binding energy 641.3 eV and 653.2 eV, while the binding energy of Mn^{4+} at 2p 3/2 and 2p 1/2 was 642.9 eV and 654.5 eV, respectively [39, 40].

The existence of various manganese valences could be conductive to the electron transfer in the NO conversion processes [39]. Via the reduction of Mn^{4+} to Mn^{3+}, lattice oxygen released. With additional lattice oxygen generated in the catalytic system, which was considered much easier and more active than the oxygen adsorbed from the mixed gas, the conversion of NO to NO_2 would be greatly improved at room temperature [36]. This was consistent with the experimental results illustrated in Figure 1.

Figure. 4 (b) and Figure. 4(c) showed the binding energy peaks of Mn 2p and Ce 3d of 10% urea-0.5CeO_2-0.5MnO_2/ACF, respectively. Mn^{3+} (641.1 eV, 652.6 eV), Mn^{4+} (642.6 eV, 654.0 eV), Ce^{3+} (886.1 eV, 904.5 eV) and Ce^{4+} (882.3 eV, 900.3 eV) [41, 42] were detected on the surface of the sample. Since electron transfer from Ce^{3+} to Ce^{4+} was much easier than that from Mn^{3+} to Mn^{4+} [23], more lattice oxygen released via the interaction between the redox couple of Ce^{4+}/Ce^{3+} and Mn^{4+}/Mn^{3+}. Therefore, NO conversion to NO_2 with 10% urea-$Ce_xMn_{1-x}O_2$/ACF was much easier than that with 10% urea-MnO_x/ACF, which resulted in higher NO conversion. This was in accord with the experimental results in Fig. 1.

Figure 5(a) and (b) were the XPS study of O 1s of 10%urea-8%MnO_x/ACF and 10%urea-0.5CeO_2-0.5MnO_2/ACF, respectively. It could be seen from Fig. 7(a) that the peak at 530.0 eV was ascribe to lattice oxygen of manganese oxide [42, 43] and the BE peak at 531.4 eV was due to hydroxyl groups [44] and the BE peak at 532.3 eV was attribute to the oxygen in C=O bond of urea [44, 45]. In Fig. 7(b), the binding energy peak of the lattice oxygen in the metal oxide was at 530.7 eV. The peak at 531.4eV and 532.8eV was corresponding to oxygen of the hydroxyl groups and the

oxygen in C=O bond of urea, respectively. It could be seen from the Fig.7 (a) and (b) that the binding energy of lattice oxygen and the oxygen in C=O bond of urea in 10%urea-0.5CeO_2-0.5MnO_2/ACF was a little higher than that in 10%urea-MnO_x/ACF. It could be concluded that the binding energy of O 1s in CeO_2 was higher than it in MnO_x and there might exist an interaction between urea and the metal oxide based on the difference of O 1s binding energy of the lattice oxygen and the oxygen in C=O bond of urea of the two samples, respectively.

3.6. XRD study

The XRD patterns of 10% urea-0.5CeO_2-0.5MnO_2/ACF were shown in Figure 6. The XRD patterns showed obvious graphite-like crystallite at 20-30^0 and 40-50^0 [13, 46]. However, there were no sharp and special visible peaks for metal oxides. This might ascribe to the reasons that the mass ratio of metal oxides loaded on ACF, about 8%, was low and metal oxides was not well crystallized on the surface of ACF. It could also be seen from the SEM image of the sample that the metal oxides were well dispersed on ACF, which might also lead to the week peaks of the XRD pattern.

After 10% urea-0.5CeO_2-0.5MnO_2/ACF reacting in the SCR process with NO for 4 h, the XRD pattern of it was almost the same as that before reaction. It demonstrated that the graphite-like crystallite changed little compared with that in its original state due to the involvement of NO in the SCR process [23, 47]. Herein, the material of 10% urea-0.5CeO_2-0.5MnO_2/ACF could be reused after urea was reloaded, which was consistent with the results showed in Fig.2.

3.7. FTIR study

To get more detailed information about the physical properties of the samples, which could greatly affect the activity of the sample in the catalytic process, FTIR experiments were conducted in this work. The results were shown in Figure 7.

In Fig.7 (a), it was apparent that chemical groups of different 10%urea-MnO_x/ACF displayed great difference as the mass ratio of manganese oxide was loaded on the 10%urea/ACF increased. Due to the modification by metal oxide, the wave number

bonds and half peak height changed. The bands of 10% urea/ACF detected were mainly at 3440 cm^{-1}, 1640 cm^{-1}, 2360 cm^{-1} and the weak bonds between 1400 cm^{-1} and 1600 cm^{-1}. The bands of 10%urea-MnO_x/ACF were primarily at 3440 cm^{-1}, 2360 cm^{-1}, 1100 cm^{-1} and 670 cm^{-1}. In Fig.7 (b), the detected bands of 10%urea-0.5CeO_2-0.5MnO_2/ACF were mainly at 3440 cm^{-1} and 2360 cm^{-1}, as well as the weak bands between 1100 cm^{-1} and 500 cm^{-1}.

In Fig. 7, the band at 3440 cm^{-1} was hydroxyl group [13, 25, 35], which was in accordance with the XPS study of the O 1s of the samples at the binding energy peak of 531.4 eV. The weak bands between 1400 cm^{-1} and 1640 cm^{-1} might be ascribed to the adsorption of NO_2 generated in the pyrolysis process , the gaseous adsorbed by ACF and the vibration of bidenate nitrate or monodenate nitrite which existed when ACF was produced [13, 25]. By comparing the FTIR graphs of different samples, the band at 2360 cm^{-1} might be attributed to the interaction between urea and metal oxide [24-25]. It could be seen from Fig. 7 that the band at 2360 cm^{-1} was very weak when urea was loaded on ACF alone. The band at 2360cm^{-1} became apparent when metal oxide and urea were both loaded on ACF. However, with urea loaded on the catalyst were exhausted after the SCR process, the band became weak again. This was consistent with the discussion in XPS study of O 1s above. The band at 2360 cm^{-1} might be beneficial to the catalytic process when manganese oxide was loaded on urea-ACF alone.

3.8. Mechanism discussion

For the selective catalysis reduction of NO with urea-MnO_x/ACF, the catalytic mechanism was discussed as below. Since the oxidation of NO to NO_2 is the key step in the reduction process of NO with urea on carbon materials as reported in previous papers [34, 37], the reduction of NO with urea would be greatly improved if the oxidation of NO could be promoted through a catalytic way. As the co-existence phenomenon of Mn^{4+} and Mn^{3+} could be found on the surface of the sample according to the XPS study of the 10% urea-8%MnO_x/ACF, it could be concluded that the

reaction of MnO_2 in the catalysis might be as below (Eq.(1)). With additional lattice oxygen produced in reaction , the oxidation of NO to NO_2 was promoted (Eq. (3)) [23].

$$2MnO_2 \leftrightarrows Mn_2O_3 + O\cdot \quad (1)$$

$$2CeO_2 \leftrightarrows Ce_2O_3 + O\cdot \quad (2)$$

$$NO + O\cdot \rightarrow NO_2 \quad (3)$$

In the XPS study of the 10%urea-0.5CeO_2-0.5MnO_2/ACF, $Ce^{4+}$and Ce^{3+} could be detected as well as Mn^{4+} and Mn^{3+}. Based on the interaction between MnO_2 and Mn_2O_3 as well as the interaction between CeO_2 and Ce_2O_3 mentioned in Eq. (2), a synergetic effect [23, 48] between manganese and cerium was expected to contribute to the promotion of the catalytic process. The interplay between cerium and manganese in the catalytic process followed the equation chains as below:

$$Mn^{4+}(ads) + NO \leftrightarrows Mn^{3+}(ads) + NO^{+}(ads) \quad (4)$$

$$Mn^{3+}(ads) + Ce^{4+}(ads) \leftrightarrows Mn^{4+}(ads) + Ce^{3+}(ads) \quad (5)$$

$$Ce^{3+}(ads) + 1/2O_2 \leftrightarrows Ce^{4+}(ads) + O^{-}(ads) \quad (6)$$

$$NO^{+}(ads) + O^{-}(ads) \rightarrow NO_2 \quad (7)$$

As urea was loaded on the samples, the interaction between urea and metal oxides placed a significant role in the system. The reaction happened on the surface of ACF involved Eq. (4)-(10). In the first place, the active sites of metal oxides were mainly occupied by urea, most NO was reduced directly by the urea at the active sites to N_2 on the surface of ACF after reaction (Eq. (8)) when the NO concentration was at a low level. As the concentration of NO increasing, the active sites of the metal oxide began to be dominant by NO. Through the reaction chains of Eq. (4)-(7), NO was converted to NO_2 which had been reported to reacts quite easily with urea on ACF [33].

There existed a competition of the active site between urea and NO, which was not that good for the reduction of NO based on the experimental results in this paper. Though both the reaction of urea in the active sites with NO and the reaction of NO_2 with urea which was not in the active site promoted the reduction of NO in the system,

the difference between the two reaction was great, even a little contrary: the reaction of urea in the active sites with NO might limit the reaction of NO_2 with urea which was not in the active site by decrease the amount of NO participated in oxidation into NO_2. NO has advantage in molecular size while competing active sizes of the metal oxides with urea.

However, when the concentration of NO was at a low level, the advantage was not that apparent and the NO conversion rate dropped with the decrease of the active site occupied by urea. When the NO concentration increased to 500 ppm, the two reactions reached an equivalent and the NO conversion rate decreased to the lowest level. With the NO concentration increased above 500 ppm, the active sites were mainly occupied by NO, and the reaction of NO_2 with urea which was not in the active site became dominant. Therefore, the NO conversion rate increased. The mechanism in this study with NO at low and high levels was similar to the Eley-Rideal mechanism and Langmuir-Hinshelwood mechanism in NH_3 SCR, respectively [1, 23-24]. However, the difference was that urea, as the reducing agent, was first loaded on the surface and not needing to be adsorbed from the mixed gases and it had advantage in occupying the active site over NO in the first place.

While in the urea/ACF system, no such competition between urea and NO existed. The catalytic oxidation of NO to NO_2 was mainly achieved by ACF and it was greatly improved as NO concentration increased. To some degree, the higher NO concentration was, the higher NO conversion to NO_2 could be achieved by ACF [49], and higher NO reduction to N_2 was attained after reaction (Eq. (8)) together with reaction (Eq. (9) and Eq. (10)).

$$4NO + O_2 + 2(NH_2)_2CO \rightarrow 4N_2 + 2CO_2 + 4H_2O \quad \Delta G_1=-1798.28KJ\ mol^{-1} \qquad (8)$$

$$2NO_2 + 2(NH_2)_2CO + O_2 \rightarrow 3N_2 + 2CO_2 + 4H_2O \quad \Delta G_2=-1410.64KJ\ mol^{-1} \qquad (9)$$

$$NO + NO_2 + (NH_2)_2CO \rightarrow 2N_2 + CO_2 + 2H_2O \quad \Delta G_3=-791.89KJ\ mol^{-1} \qquad (10)$$

3.9. Kinetic discussion

The pseudo-first order rate constant (k) could be calculated through the equation

[11-12, 33]:

$$k = -\frac{F}{W}\ln(1-S) \quad (11)$$

In the equation, F was the total rate (ml/s), W was the mass of the catalyst (g) and S was the ratio of NO conversion.

As mentioned above, the adsorption of the urea on the catalyst follows Eq. (12-16) [11-12]:

$$(NH_2)_2CO \leftrightarrows (NH_2)_2CO^* \quad (12)$$

$$(NH_2)_2CO^* + \equiv M^{4+} \rightarrow -NH_2 + \equiv M^{3+} + NH_2CO^+ \quad (13)$$

$$NH_2CO^+ + \equiv M^{4+} + O^{2-} \rightarrow -NH_2 + \equiv M^{3+} + CO_2 \quad (14)$$

$$-NH_2 + NO(g) \rightarrow N_2 + H_2O \quad (15)$$

$$\equiv M^{3+} + 1/4O_2 \rightarrow \equiv M^{4+} + 1/2\equiv O^{2-} \quad (16)$$

In the equation above, * expresses the molecular adsorbed on the surface of the catalyst and M represents manganese and cerium.

The kinetic equation of reaction (15) could be written as below:

$$-\frac{d[-NH_2]}{dt} = -\frac{d[NO_{(g)}]}{dt} = \frac{d[N_2]}{dt} = k_1[-NH_2][NO_{(g)}] \quad (17)$$

In which k_1 was the kinetic constant of reaction (15).

In reaction (13) and reaction (14), when the surface of catalyst was saturated with the adsorption of $-NH_2$, $[-NH_2]$ could be viewed as a constant which could be approximately written as:

$$[-NH_2] = [M^{4+}]\{k_2[(NH_2)_2CO^*] + k_3[NH_2CO^+]\} \quad (18)$$

k_2 and k_3 were constants in the equation. $[M^{4+}]$ was the concentration of reducible M^{4+}, was the kinetic constant.

Therefore, based on the kinetic equation above, it could obtain the flowing equation:

$$\int \frac{d[NO_{(g)}]}{[NO_{(g)}]} = -\int k_1\{k_2[(NH_2)_2CO^*] + k_3[NH_2CO^+]\}[M^{4+}]\,dt \quad (19)$$

$$\int_{[NO_{(g)}]_{in}}^{[[NO_{(g)}]_{t'}]} \frac{d[NO_{(g)}]}{[NO_{(g)}]} = -\int_0^{t'} k_1\{k_2[(NH_2)_2CO^*] + k_3[NH_2CO^+]\}[M^{4+}]dt \quad (20)$$

$[NO_{(g)}]_{in}$ was the NO concentration at the very beginning. Therefore, the gaseous

NO concentration at the specific part of the catalyst column ($[NO_{(g)}]_{t'}$) could be written as:

$$[NO_{(g)}]_{t'}= [NO_{(g)}]_{in} \exp(-k_1\{k_2[(NH_2)_2CO^*]+k_3[NH_2CO^+]\}[M^{4+}]t') \quad (21)$$

t' in the equation represent the time it took for NO to reach the specific part of catalyst column. The whole kinetic equation could be written as:

$$-\frac{d[NO_{(g)}]}{dt}$$

$$=\int_0^{t^*} d[NO_{(g)}]_{t'}=\int_0^{t^*} k_1\{k_2[(NH_2)_2CO^*] + k_3[NH_2CO^+]\}[M^{4+}] [NO_{(g)}]_{t'}dt' \quad (22)$$

$$=k_1\{k_2[(NH_2)_2CO^*]+k_3[NH_2CO^+]\}[M^{4+}][NO_{(g)}]_{in}\times\int_0^{t^*} k_1\{k_2[(NH_2)_2CO^*] +$$

$$k_3[NH_2CO^+]\}[M^{4+}] t')dt'$$

t* was a constant, which was equal to the reciprocal of GHSV.

As the NO concentration increasing, the reaction chains bellow become dominant:

$$(NH_2)_2CO \leftrightarrows (NH_2)_2CO^* \quad (12)$$

$$NO_{(g)} \leftrightarrows NO^* \quad (23)$$

$$NO^*+\equiv M^{4+}+O^{2-}\rightarrow NO_2^-+\equiv M^{3+} \quad (24)$$

$$NO_2^-+ (NH_2)_2CO^* \rightarrow N_2+2OH^-+NH_2CO^+ \quad (25)$$

$$NO_2^-+NH_2CO^+ \rightarrow N_2+H_2O +CO_2 \quad (26)$$

$$\equiv M^{3+}+1/4O_2\rightarrow\equiv M^{4+}+1/2\equiv O^{2-} \quad (27)$$

The concentration of NO in the mixed was adequately high for the saturation of its adsorption on the surface, especially in the supported system in which ACF could serve as a reservoir for NO. Therefore, the concentration of NO^* [NO^*] was a constant. The reaction of NO_2^- with $(NH_2)_2CO^*$ and NH_2CO^+ in reaction (25) and (26) could be equivalent to the reaction of NO_2^- with $-NH_2^*$. Then, reaction (25) and reaction (26) could be described as:

$$NO_2^-+ -NH_2^* \rightarrow N_2+2OH^- \quad (28)$$

The concentration of $-NH_2^*$[$-NH_2^*$] was proportional to [$(NH_2)_2CO^*$] and

$[NH_2CO^+]$:

$$[\text{-}NH_2{}^*]=k_4\ \{k_5\,[(NH_2)_2CO^*]+k_6\,[NH_2CO^+]\} \quad (29)$$

k_4, k_5, k_6 were constants in the equation.

The kinetic equations of reaction (24), (28) could be described as:

$$-\frac{d[NO^*]}{dt}=-\frac{d[M^{4+}]}{dt}=\frac{d[NO_2^-]}{dt}=k_7\,[NO^*]\,[M^{4+}] \quad (30)$$

$$-\frac{d[NO_2^-]}{dt}=-\frac{d[-NH_2{}^*]}{dt}=\frac{d[N_2]}{dt}=k_8\,[NO_2^-]\,[\text{-}NH_2{}^*] \quad (31)$$

In the equation, k_7, k_8 were the kinetic constant of reaction (24) and (28), respectively. $[NO_2^-]$ was the concentration of NO_2^- and $[M^{4+}]$ was the concentration of reducible M^{4+}, both of them were kinetic constants. When the chemical adsorption of NO_2^- was saturated on the surface, $[NO_2^-]$ became an invariable:

$$[NO_2^-]=\int_0^t k_7[NO^*]\,[M^{4+}]dt=k_9\,[NO^*]\,[M^{4+}] \quad (32)$$

In Eq(32), k_9 was a constant in the equation, which related to the oxidation of NO^* in reaction (24). Then equation (31) could be further described as:

$$-\frac{d[NO_2^-]}{dt}=-\frac{d[-NH_2{}^*]}{dt}=\frac{d[N_2]}{dt}$$
$$=k_4\,k_8\,k_9\,[NO^*]\,[M^{4+}]\ \{k_5\,[(NH_2)_2CO^*]+k_6\,[NH_2CO^+]\} \quad (33)$$

Hence the catalytic reduction of NO could be integrated as:

$$-\frac{d[NO_{(g)}]}{dt}=k_4\,k_8\,k_9\,[NO^*]\,[M^{4+}]\ \{k_5\,[(NH_2)_2CO^*]+k_6\,[NH_2CO^+]\}\ t^* \quad (34)$$

In which t* was the reciprocal of GHSV.

Therefore, it could be concluded from the kinetic discussion that the catalytic efficiency of NO was greatly affected by BET surface area of the samples and the catalytic reactivity of the transition metal oxide. With high BET area and catalytic ability, large amount of NO* or $(NH_2)_2CO$* could be generated in the purification procession. Moreover, the generated NO* or $(NH_2)_2CO$* was quickly take part in the purifying reactions of NO which resulted in the significantly enhancement on the NO conversion. It was consistent with the experimental results.

4. Conclusions

In this study, a reusable material with high performance for NO purification is prepared. When ACF loads urea and Mn-Ce mixed oxides, high NO conversion can be achieved at room temperature. The urea-0.5CeO_2-0.5MnO_2/ACF shows the highest catalytic activity among all of the prepared materials due to its super synergetic effect between manganese and cerium. Moreover, the NO concentration can greatly influence the NO conversion. When the NO concentration is 100 ppm, over 98% NO conversion can be yielded by urea-0.5CeO_2-0.5MnO_2/ACF. Specially, the material of 10%urea-0.5CeO_2-0.5MnO_2/ACF can be re-robust by reloading urea when it is useless on purifying NO at room temperature. Therefore, the material studied in this work is efficient enough to remove NO from atmospheric environment at room temperature, where the NO concentration was usually below 100 ppm.

Acknowledgement

This work was supported by the Joint Funds of the National Natural Science Foundation of China (Grant No.U1560110), the National Natural Science Foundation of China (Grant No.51108169) and Fundamental Research Funds for the Central Universities.

Reference

[1] G.S. Qi, R. T. Yang. J. Catal., 2003,**217**, 434.

[2] C. E. Stere, W. Adress, R. Burch, S. Chansai, A. Goguet, W. G. Graham, F. De Rosa, V. Palma, C. Hardacre, ACS Catal. 2014, **4**, 666.

[3] D. L. TorreUnai, P.-A. Beñat, G.-V. Juan R. Chem. Eng. J., 2012,**207–208**, 10.

[4] X. Wang, W. Wen, J. Mi, X. Li, R. Wang, Appl. Catal. B: Environ. 2015, **176–177**, 454.

[5] C.N. Costa, A.M. Efstathiou, Appl. Catal. B: Environ., 2007,**72**, 240.

[6] J.H. Li, Y.Q. Zhu, R. Ke, J.M. Hao, Appl. Catal. B: Environ., 2008,**80**, 202.

[7] P. Sazama, L. Čapek, H. Drobná, Z. Sobalík, J. Dědeček, K. Arve, B. Wichterlová.

J. Catal., 2005,**232**, 302.

[8] Y. J. Kim, J. K. Lee, K. M. Min, S. B. Hong, I.-S. Nam, B. K. Cho, J. Catal. 2014, **311**, 447.

[9] T. Boningari, P. R. Ettireddy, A. Somogyvari, Y. Liu, A. Vorontsov, C. A. McDonald, P. G. Smirniotis, J. Catal. 2015, **325**, 145.

[10] M. Yasuda, N. Tsugita, K. Ito, S. Yamauchi, W. R. Glomm, I. Tsuji, H. Asano, Environ. Sci. Technol. 2011, **45**, 1840.

[11] S.J. Yang, C.Z. Wang, J.H. Li, N.Q. Yan, L. Ma, H.Z. Chang. Appl. Catal. B: Environ., 2011, **110**, 71.

[12] S.J. Yang, J.H. Li, C.Z. Wang, J.H. Chen, L. Ma, H.Z. Chang, L. Chen, Y. Peng, N.Q. Yan. Appl. Catal. B: Environ., 2012, **117-118**, 73.

[13] P. Lu, C.T Li, G.M. Zeng, L.J. He, D.L. Peng, H.F. Cui, S.H. Li, Y.B. Zhai. Appl. Catal. B: Environ., 2010,**96**, 157.

[14] C.T. Li, P. Lu, G.M. Zeng, Q.J. Wang, Q. Li, L.J. He, Y.B. Zhai. Chinese J. Environ. Sci., 2008,**29**, 3280.

[15] L. Gutierrez, E. A. Lombardo. Appl. Catal. A: Gen., 2009,**360**, 107.

[16] P.S. Metkar, N. Salazar, R. Muncrief, V. Balakotaiah, M.P. Harold, Appl. Catal. B: Environ., 2011, **104**, 110.

[17] P. Sazama, B. Wichterlová, E. Tábor, P. Šťastný, N. K. Sathu, Z. Sobalík, J. Dědeček, Š. Sklenák, P. Klein, A. Vondrová, J. Catal. 2014, **312**, 123.

[18] Z. Zeng, P. Lu, C.T. G.M. Zeng, X. Jiang. J. Coord. Chem., 2012**,65**, 1992.

[19] J.H. Huang, Z.Q. Tong, Y. Huang, J.F. Zhang. Appl. Catal. B: Environ.,2008,**78**, 309.

[20] Y.S. Shen, S.M. Zhu, T. Qiu, S.B. Shen. Catal. Commun., 2009,**11**, 20.

[21] H. Li, X.L. Tang, H.H. Yi, L.L. Yu. J. Rare Earth., 2010,**28**, 64.

[22] K. Tikhomirov, O. Krocher, M. Elsener, A. Wokaun, Appl. Catal. B: Environ.,2006,**64**, 72.

[23] G.S. Qi, R.T. Yang, R. Chang, Appl. Catal. B: Environ., 2004,**51**, 93.

[24] G.S. Qi, R.T. Yang, J. Phys. Chem. B., 2004,**108**, 15738.

[25] B.X. Shen, H.Q. Ma, Y. Yao. J. Environ. Sci. , 2012, **24**, 499.

[26] U. Diebold, Surf. Sci. Rep., 2003,**48**, 53.

[27] J. Miyawaki, T. Shimohama, N. Shimohama, A. Yasutake, M. Yoshikawa, I. Mocjida, S-H. Yoon. Appl. Catal. B: Environ., 2011, **110**, 273.

[28] A. Trapalis, N. Todorova, T. Giannakopoulou, N. Boukos, T. Speliotis, D. Dimotikali, J. Yu, Appl. Catal. B: Environ. 2016, **180**, 637.

[29] Q. Yu, H. Wang, T. Liu, L. Xiao, X. Jiang, X. Zheng, Environ. Sci. Technol. 2012, **46**, 2337.

[30] Z. Zeng, P. Lu, C.T. Li, L. Mai, Z. Li and Y.S. Zhang. Catal. Sci. Technol., 2012, **2**, 2188.

[31] J.S. Moon, K.K. Park, J.H. Kim, G. Seo, Appl. Catal. A:Gen., 1999,**184**, 41.

[32] M Koebel, M Elsener, M Kleemann. Catal. Today, 2000,**59**, 335.

[33] N. Shirahama, I. Mochida, Y. Korai, K.H. Choi, T. Enjoji, T. Shimohara, A. Yasutake, Appl. Catal. B: Environ.,2004,**52**, 173.

[34] P. Lu, Z. Zeng, C.T. Li, G.M. Zeng, J. Guo, X. Jiang, Y.B. Zhai, X.P. Fan. Environ. Technol., 2012,**33**, 1029.

[35] Z. Zeng, P. Lu, C.T. Li, G.M. Zeng, X. Jiang, Y.B. Zhai, X.P. Fan. Environ. Technol., 2012,**33**, 1331.

[36] X. Jiang, P. Lu, C.T. Li, Z. Zeng, G.M. Zeng, L.P. Hu, L. Mai, Z. Li. Environ. Technol.,2013, 34 (5), 591-598.

[37] N. Shirahama, I. Mochida, Y. Korai, K.H. Choi, T. Enjoji, T. Shimohara, A. Yasutake, Appl. Catal. B: Environ.,2005,**57**, 237.

[38] M. Molina-Sabio, M.T. Gonzalez, F. Rodriguez-Reinoso, A. Sepúlveda-Escribano, Carbon, 1996, **34**, 505.

[39] S. M. Lee, K. H. Park, S. C. Hong. Chem. Eng. J., 2012,**195–196,** 323.

[40] W.J. Hong S. Iwamoto, S. Hosokawa, K. Wada, H. Kanai, M. Inoue. J. Catal., 2011,**277**, 208.

[41] P. Li, P. Lu, Y.Zhai, C. Li, T. Chen, R. Qing, W. Zhang. Environ. Technol. 2015, **18** 2390.

[42] Shi L, Chu W, Qu F, Luo, S. Catal.Lett., 2007, **113**, 59.

[43] M. Machida, M. Uto and D. Kurogi, Chem. Mater. 2000, **12**, 3158.

[44] Alifanti, M., Baps, B., Blangenois, N., Naud, J., Grange, P., &Delmon, B. Chem. Mater. 2003,**15**, 395.

[45] Moulder, J. F.; Sticle, W. F.; Sobol, P. E.; Bomben, K. D. Handbook of XPS; Chastain, J., Ed.; Perkin-Elmer Corporation: Wellesley, MA 1992

[46] L.L. Zhu, B.C. Huang, W.H. Wang, Z.L. Wei, D.Q. Ye. Catal. Commun.,2011, **12**,394.

[47] M.A. Daley, D. Tandon, J. Economy, E.J. Hippo. Carbon, 1996,**34**, 1191.

[48] G. Carja, Y. Kameshima, K. Okada, C. D. Madhusoodana. Appl. Catal. B: Environ., 2007, **73**, 60.

[49] S. Adapa, V. Gaur , N. Verma. Chem. Eng. J., 2006, **116**, 25.

Figure captions

Figure 1 SCR activity of NO of the prepared materials:

a) 10%urea-MnO_x/ACF;

b) 10%urea-xCeO_2-(1-x)MnO_2/ACF

Figure 2 Stability of 10%urea-0.5CeO_2.0.5MnO_2/ACF for NO purification

Figure 3 Effect of NO concentrations on its removal by 10%urea-0.5CeO_2-0.5MnO_2/ACF

Figure 4 XPS results:

a) Mn 2p 1/2 and 2p 3/2 scan results of 10%urea-8%MnO_x/ACF;

b) Mn 2p 1/2 and2p 3/2 scan result of 10%urea-0.5CeO_2-0.5MnO_2/ACF;

c) Ce 3d 3/2 and 3d 5/2 scan result of 10%urea-0.5CeO_2-0.5MnO_2/ACF

Figure 5 XPS experimental results O 1s:

a) 10%urea-8%MnO_x/ACF;

b)10%urea-0.5CeO_2-0.5MnO_2/ACF

Figure 6 XRD experimental results of 10%urea-0.5CeO_2-0.5MnO_2/ACF

Figure 7 FTIR experimental of prepared catalysts

a) 10%urea-MnO_x/ACF

b) 10%urea-0.5CeO_2-0.5MnO_2/ACF

Figures

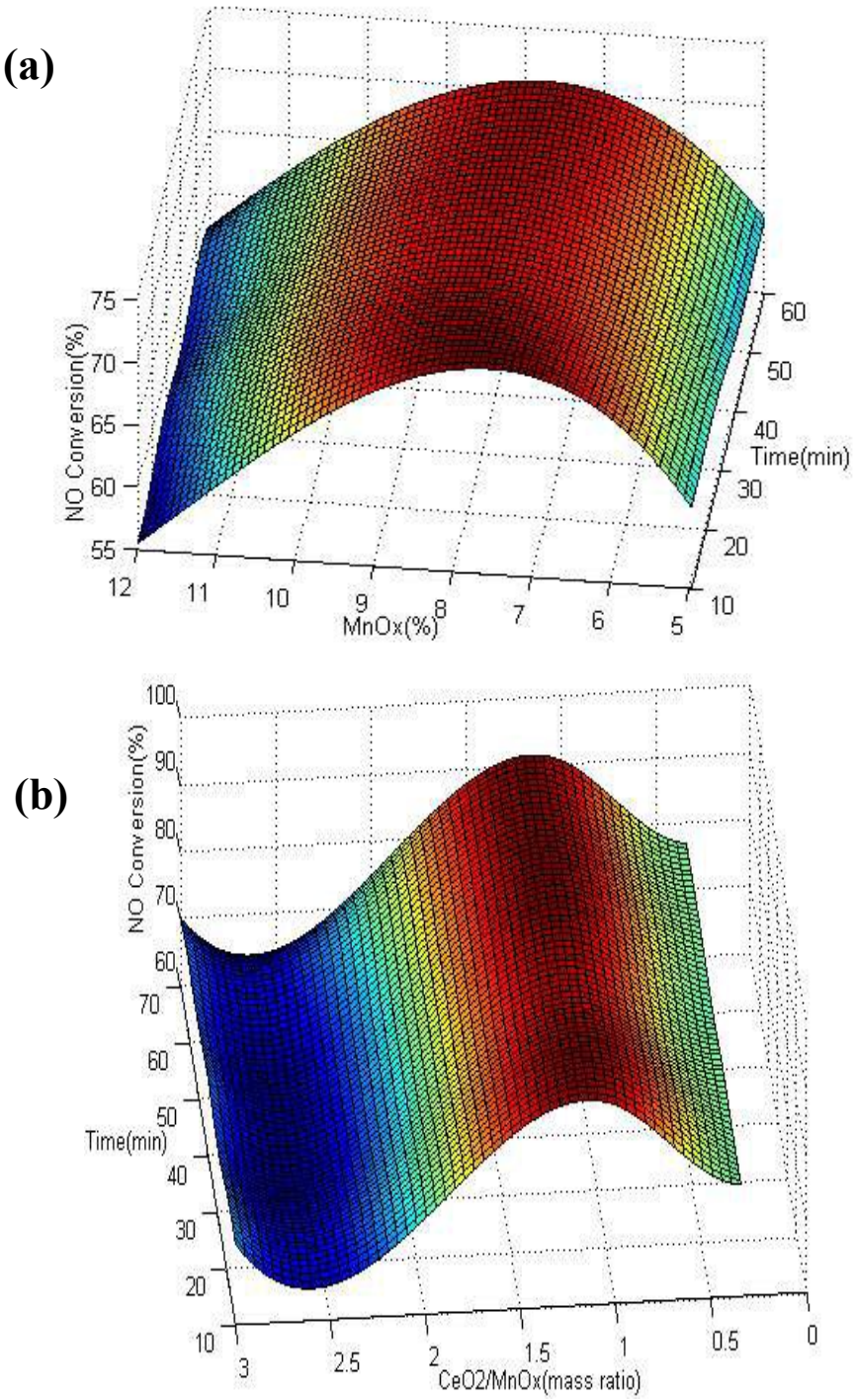

Figure1 SCR activity of NO of the prepared samples: a)10%urea-MnO_x/ACF b)10%urea- $xCeO_2$-(1-x) MnO_2/ACF

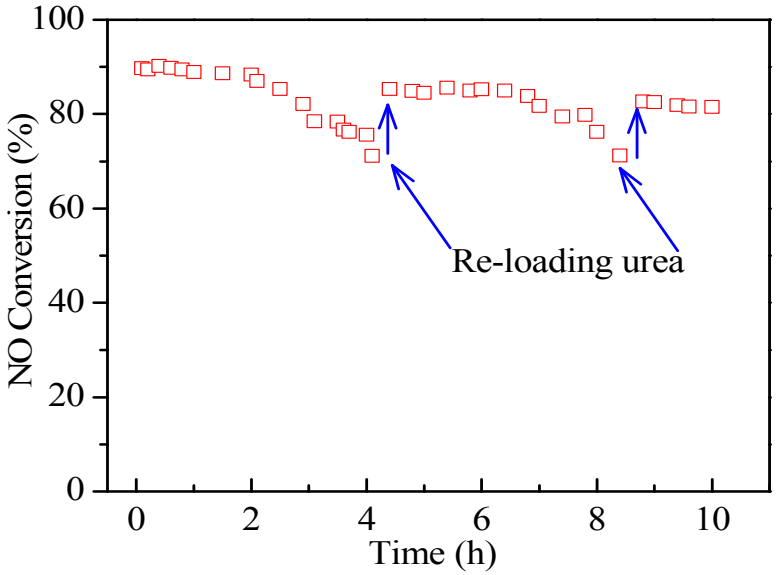

Figure 2 SCR stability of NO of 10%urea-0.5CeO_2-0.5MnO_2/ACF

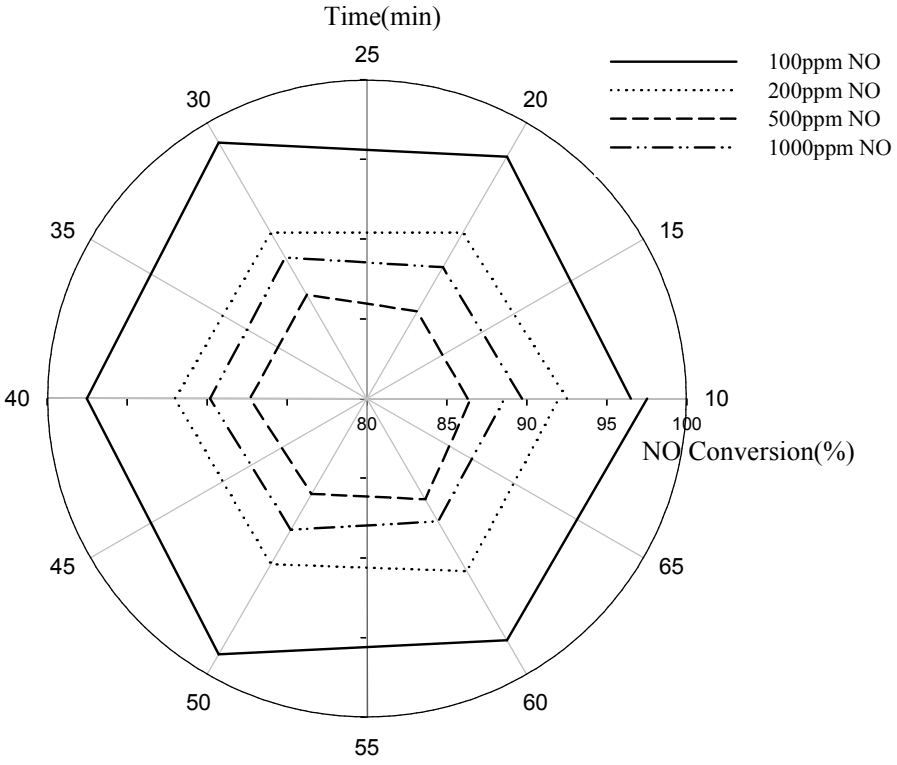

Figure 3 Effect of NO concentrations on its removal by 10%urea-0.5CeO_2-0.5MnO_2/ACF

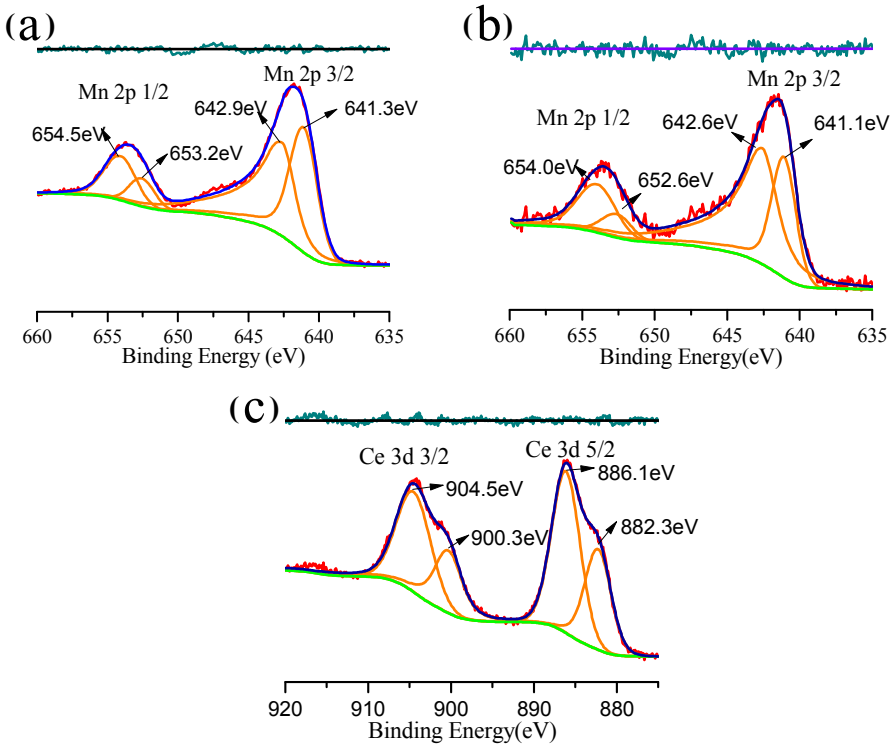

Figure 4 XPS results: (a) Mn 2p 1/2 and 2p 3/2 scan result of 10%urea-8%MnO_x/ACF; (b) Mn 2p 1/2 and2p 3/2 scan result of 10%urea-0.5CeO_2-0.5MnO_2/ACF; (c) Ce 3d 3/2 and 3d 5/2 scan result of 10%urea-0.5CeO_2-0.5MnO_2/ACF

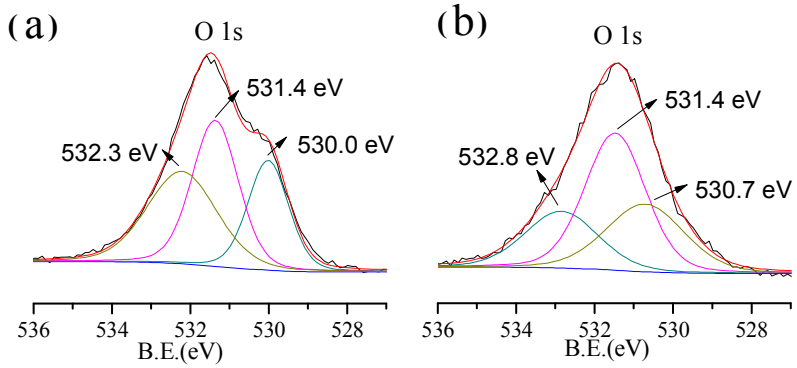

Figure 5 XPS experimental results of O 1s: (a) 10%urea-8%MnO_x/ACF;

(b) 10%urea-0.5CeO_2-0.5MnO_2/ACF

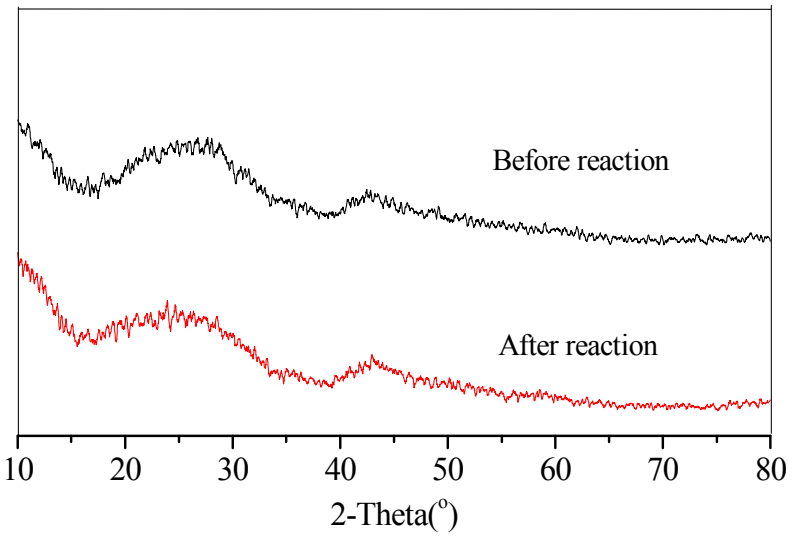

Figure 6 XRD experimental results of 10%urea-0.5CeO_2-0.5MnO_2/ACF

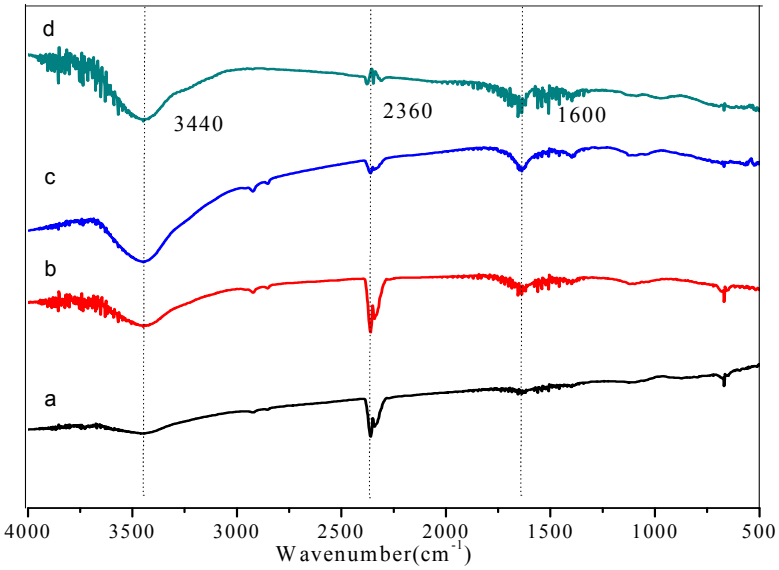

(a) 10%urea-MnO_x/ACF

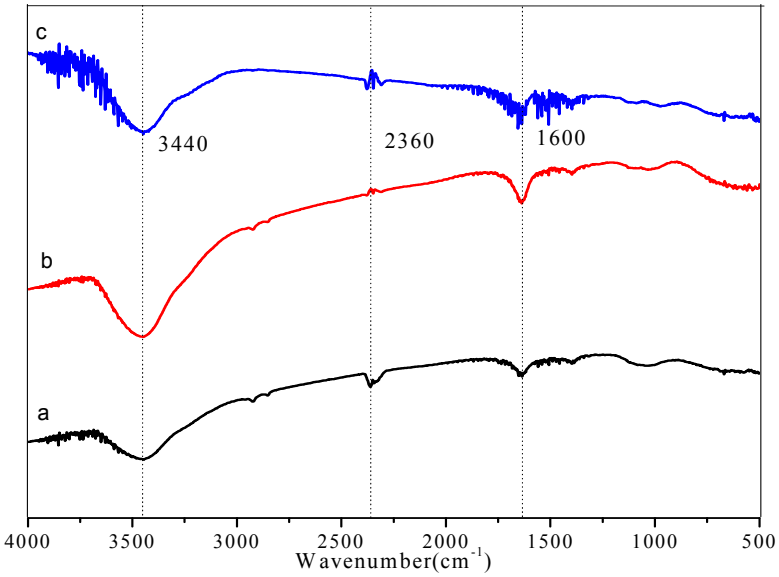

(b)10%urea-0.5CeO_2-0.5MnO_2/ACF

Figure 7 FTIR experimental results of prepared catalysts

Table:

Table 1 Values of surface areas, pore volumes and pore size of the catalysts

Sample	$S_{BET}(m^2/g)$	$S_{meso}(m^2/g)$	$S_{micro}(m^2/g)$	$V_t(cm^3/g)$	$V_{micro}(cm^3/g)$	D_A (nm)
ACF	1491.23	751.72	739.51	0.71	0.34	19.16
10%urea-5%MnO_X/ACF	1447.39	769.66	677.73	0.69	0.31	19.20
10%urea-8%MnO_X/ACF	1386.59	642.86	743.73	0.66	0.34	19.21
10%urea-10%MnO_X/ACF	1339.34	624.28	715.06	0.64	0.33	19.21
10%urea-0.5CeO_2-0.5MnO_2/ACF	1234.42	605.76	628.66	0.60	0.29	19.36

Table 2 At% of detected elements on the surface of catalysts

Sample	Element			
	Mn 2p	Ce 3d	O 1s	N 1s
10%urea-8%MnO_x/ACF	20.5	-	55.8	13.5
10%urea-0.5CeO_2-0.5MnO_2/ACF	4.3	9.3	45.3	33.4

Graphical Abstract: